THE JOURNAL OF BIOLOGICAL CHEMISTRY VOL. 282, NO. 48, pp. 35247–35258, November 30, 2007
Printed in the U.S.A.

Cellular Expression and Crystal Structure of the Murine Cytomegalovirus Major Histocompatibility Complex Class I-like Glycoprotein, m153*[S]

Received for publication, August 14, 2007, and in revised form, September 13, 2007 Published, JBC Papers in Press, September 26, 2007, DOI 10.1074/jbc.M706782200

Janet Mans[‡§1], Kannan Natarajan[‡], Andrea Balbo[‖], Peter Schuck[‖], Daniel Eikel[**], Sonja Hess[‡‡], Howard Robinson[§§], Hrvoje Šimić[¶¶], Stipan Jonjić[¶¶], Caroline T. Tiemessen[§¶2], and David H. Margulies[‡3]

From the [‡]Molecular Biology Section, Laboratory of Immunology, NIAID and [‖]Office of the Director, National Institutes of Health, Bethesda, Maryland 20892, the [**]Product Application Laboratory, Advion BioSystems, Ithaca, New York 14850, the [‡‡]Proteome Exploration Laboratory, Beckman Institute, California Institute of Technology, Pasadena, California 91125, the [§§]Brookhaven National Laboratory, Upton, New York 11973, the [¶¶]Department of Histology and Embryology, Faculty of Medicine, University of Rijeka, Rijeka 51000, Croatia, the [§]Department of Virology, University of the Witwatersrand, Johannesburg 2050, South Africa, and the [¶]National Institute for Communicable Diseases, Sandringham 2131, South Africa

Mouse cytomegalovirus (MCMV), a β-herpesvirus that establishes latent and persistent infections in mice, is a valuable model for studying complex virus-host interactions. MCMV encodes the m145 family of putative immunoevasins with predicted major histocompatibility complex, class I (MHC-I) structure. Functions attributed to some family members include down-regulation of host MHC-I (m152) and NKG2D ligands (m145, m152, and m155) and interaction with inhibitory or activating NK receptors (m157). We present the cellular, biochemical, and structural characterization of m153, which is a heavily glycosylated homodimer, that does not require β2m or peptide and is expressed at the surface of MCMV-infected cells. Its 2.4-Å crystal structure confirms that this compact molecule preserves an MHC-I-like fold and reveals a novel mode of dimerization, confirmed by site-directed mutagenesis, and a distinctive disulfide-stabilized extended N terminus. The structure provides a useful framework for comparative analysis of the divergent members of the m145 family.

A major strategy for immune evasion, employed by the large DNA viruses like herpes- and poxviruses, is the expression of a variety of molecules that attenuate the host's immune response. Some of these impair the cellular pathways of antigen processing and presentation, whereas others serve as decoys, mimicking host molecules crucial to natural killer (NK)[4] or T-cell recognition (1). The genome of MCMV, which serves as a model for the human virus (HCMV), encodes a set of proteins that are predicted to be structural analogs of class I major histocompatibility (MHC-I) glycoproteins (2–4). The detailed function of each of these viral MHC-I-like molecules (MHC-Iv) has not yet been determined, but several examples suggest that they either down-regulate host MHC-I or MHC-I-like molecules or directly bind to NK-cell inhibitory receptors. Thus, they can interfere with key components of T-cell recognition or NK-cell activation, thereby promoting virus survival. MHC-I molecules, transmembrane cell surface receptors consisting of a heavy chain, a β2-microglobulin (β2m) light chain, and bound peptides, are poised for recognition by clonotypic αβ receptors on $CD8^+$ T cells or by inhibitory or activating receptors on NK cells. MHC-I are classic (Ia) or non-classic (Ib) molecules based on their amino acid sequence polymorphism, function, and tissue-specific expression. The heavy chain consists of an α1α2 domain unit containing two α-helices set atop an eight-stranded β-sheet platform and an Ig-like α3 domain (5). MHC-Ib molecules exhibit less polymorphism, most do not bind peptide, and they vary in their association with β2m (6). MHC-Ib proteins function both in immune recognition and in other physiological settings (7).

Only one MCMV protein, m144, like its HCMV counterpart UL18 (8), is clearly related to MHC-I based on amino acid sequence similarity (9). m144 allows virus-infected cells to evade the NK cell response, but its mechanism of action and the nature of any ligand remain unclear. Expression studies of m144 indicate that, unlike MHC-Ia molecules, it does not require peptide for cell surface expression (10, 11). The crystal structure of m144 reveals an MHC-I-like protein, bound to β2m but not associated with peptide, confirming predictions based on sequence comparison. The molecule is characterized

* This work was supported in part by the Intramural Research Program of NIAID and NIDDK, National Institutes of Health. The costs of publication of this article were defrayed in part by the payment of page charges. This article must therefore be hereby marked "*advertisement*" in accordance with 18 U.S.C. Section 1734 solely to indicate this fact.

The atomic coordinates and structure factors (code 2O5N) have been deposited in the Protein Data Bank, Research Collaboratory for Structural Bioinformatics, Rutgers University, New Brunswick, NJ (http://www.rcsb.org/).

[S] The on-line version of this article (available at http://www.jbc.org) contains supplemental "Experimental Procedures," Figs. S1–S5, and Table S1.

[1] Supported by a predoctoral fellowship from the National Institutes of Health and the Polio Research Foundation of South Africa.

[2] Recipient of a Wellcome Trust senior international research fellowship (076352/Z/05/Z).

[3] To whom correspondence should be addressed: Molecular Biology Section, Laboratory of Immunology, NIAID, 10 Center Dr., Bethesda, MD 20892-1892. Tel.: 301-496-6429; Fax: 301-496-0222; E-mail: dhm@nih.gov.

[4] The abbreviations used are: NK, natural killer; MHC-I, major histocompatibility class I; MCMV, mouse cytomegalovirus; HCMV, human cytomegalovirus; TAP, transporter associated with antigen processing; SeMet, selenomethionine; SAD, single anomalous dispersion; r.m.s.d., root mean square deviation; p.i., post infection; SEC, size exclusion chromatography; BiFC, bimolecular fluorescence complementation; YFP, yellow fluorescent protein; FACS, fluorescence-activated cell sorting; GFP, green fluorescent protein; mAb, monoclonal antibody; HA, hemagglutinin; TLS, translation, libration, screw; NCS, non-crystallographic symmetry.

by a large angle between α1α2 and α3, a unique stabilizing disulfide bond in α1α2, and relatively loose association of the heavy chain with β2m (11).

In addition to m144, MCMV encodes the eight molecules of the m145 family, all of which are predicted to have an MHC-I protein fold (2–4), despite the lack of significant sequence similarity to m144 or to MHC-Ia molecules. Four of the family members (m145, m152, m155, and m157) function as immunoevasins. m145, m152, and m155 down-regulate the cell surface expression of ligands of the activating receptor NKG2D (12–15). m152 also causes the retention of MHC-I molecules in the endoplasmic reticulum-Golgi intermediate compartment (16). m157 functions by binding the NK inhibitory receptor $Ly49I^{129}$ in MCMV-sensitive mouse strains such as 129. Alternatively it can interact with the NK-activating receptor Ly49H in strains (*e.g.* C57BL/6) that are resistant to MCMV infection (2, 17). m157 expression requires neither β2m nor peptide (2). Its crystal structure revealed several deviations from the MHC-Ia fold: an extended, helical N terminus, designated α0, that precedes the canonical α1 helix and imparts a three-helix structure to the N-terminal α1α2 domain; a long α2 helix that extends into the α3 domain; short interhelical distances and close interactions of the α1α2 domain with α3 resulting in a molecule significantly more compact than classic MHC-I; and an α3 domain whose Ig fold is less twisted than typical Ig folds (18).

The unique functions of m145, m152, m155, and m157 suggest that each member of the m145 family is important in modulating the response of the host to MCMV infection. The structural features of m144 and m157 imply that other members of the m145 family also may have evolved significant structural deviations from typical MHC-I to solve novel difficulties in their encounter with the immune system. An understanding of the evolution and function of the MHC-I-like molecules of MCMV demands examination of the cellular expression, immunological function, and molecular structure of each of these molecules. To gain further insight into another member of the m145 family, we have examined m153 in detail. We first demonstrate that *m153* is a functional gene that directs the expression of its encoded protein to the surface of MCMV-infected cells. Surface expression is independent of the transporter associated with antigen processing (TAP) or β2m. In surprising contrast to MHC-I molecules, recombinant soluble m153 is homodimeric. The crystal structure of m153 described here reveals the mode of dimerization in addition to other distinguishing features. Thus, although prediction algorithms group members of the m145 family together within the broad MHC-I structural family, the details of the individual structures show wide variation from MHC-I and demonstrate the robustness and adaptability of the MHC-I fold in the service of diverse biological functions.

EXPERIMENTAL PROCEDURES

Cell Lines

NIH3T3, RMA, and RMA-S were grown in Dulbecco's modified Eagle's medium containing 10% fetal bovine serum, 5×10^{-5} M 2-mercaptoethanol, 1× non-essential amino acids (BioWhittaker), and 50 μg/ml gentamicin at 37 °C in 5% CO_2. R1.1 and R1E were cultured in RPMI containing the same supplements as above. *Drosophila* S2 cells were maintained in Insect Express medium (BioWhittaker) supplemented with 50 μg/ml gentamicin except where mentioned otherwise.

Antibodies

Rabbit antiserum was produced against m153 expressed as inclusion bodies in *Escherichia coli*. Reduced, denatured SDS-gel-purified m153 was emulsified in complete Freund adjuvant prior to immunization. The mouse monoclonal antibody mAb153.16, generated with the extracellular domain of mature m153 (amino acids 1–314) expressed in S2 cells, stains m153-transfected cells and immunoprecipitates m153 from transfected or virus-infected cells.

Vector Constructs

Insect Cell Expression—cDNA encoding the extracellular domain of the mature form of m153 (amino acids 1–314) was PCR-amplified from MCMV-infected cell culture supernatants (Smith strain, American Type Culture Collection, catalog no. VR-1399) using primers 5′*GGATCC*GAGGTCGTGCGGCCCGAAGTTAAC and 5′*GGTACC*TCAATGGTGATGGTGATGATGGCTGCCGCGCGGCACCAGGGTCAGTCTCGAATCGTTGATCGTC. A BamHI restriction site was incorporated into the forward primer, and a thrombin cleavage site (LVPRG), a His_6 tag, a termination codon, and a KpnI restriction site were incorporated into the reverse primer. The m153 PCR product was directly cloned into the pCR4-Topo-TA vector (Invitrogen), the sequence was verified, and then the excised BamHI/KpnI m153 fragment was inserted in the BglII and KpnI sites of pMT-Bip-V5-His (Invitrogen).

Mammalian Cell Expression—The full-length *m153* gene (encoding amino acids −22–382, including the signal peptide sequence) was amplified from MCMV-infected cell culture supernatants and an N-terminal FLAG tag introduced by sequential PCR. The sequential forward primers used were: A, 5′TCAGCGGAGGTCGACTACAAGGATGACGATGACAAGGTGCGGCCCGAAGTTAACAGG; B, 5′TTGGTTCTCATCTCAGGAGGGTTCTGGGCGTGCGGCTCAGCGGAGGTCGACTACAAG; and C, 5′GCTAC*GGGATCC*ATGATTCCCCTTCTCCTTCTGCCGTTGGTTCTCATCTCAGGAGGG. The reverse primer was 5′TACGCT*GAATTC*TTACACCACATTCTCCTCCGTATCCGAGCA. 5′ BamHI and a 3′ EcoRI restriction sites were incorporated in the forward and reverse primers, respectively, for subsequent cloning into the pIRES-hrGFP-II vector (Stratagene).

BiFC Vectors

Mammalian expression vectors encoding the N-terminal 1–154 residues (N-YFP) or the C-terminal 155–238 residues (C-YFP) of YFP were a kind gift from Dr. K. Ozato, NICHD, National Institutes of Health. m153 and m144 were amplified from existing full-length constructs using primers m153_5YFP (5′AC*GGGATCC*ATGATTCCCCTTCTCCTTCTGCCG) and m153_3YFP (5′AC*GGAATTC*GCCACCACATTCTCCTCCGTATCCG), and m144 was amplified using primers m144_5YFP (5′AC*GAGATCT*ATGAGGGCTCTGGCGCTG) and m144_3YFP (5′AC*GGAATTC*GCAATGCTGGGATCC-

GGGACCGTG). The PCR products were digested and inserted into the BglII and EcoRI sites of N-YFP and C-YFP, and the sequences were verified. The resulting constructs encode fusion proteins of m153 and m144 linked at their C termini to either the N- or C-terminal fragments of YFP. A 12- to 13-amino acid spacer separates the viral proteins from the YFP fragments.

β2m and TAP Dependence

The Amaxa nucleofector (Amaxa Biosystems) was used to introduce the pIRES-hr-GFP II vector (Stratagene) encoding either FLAG-m153 or H-2D^d into R1.1 and R1E cells (solution V, program A30) or into RMA and RMA-S cells (solution T, program A30) according to the manufacturer's instructions. 18–24 h post transfection the cells were stained for surface expression of FLAG-tagged m153 with the M2 monoclonal antibody (Sigma) and a phycoerythrin-labeled anti-mouse IgG_1 antibody (Southern Biotech). H-2D^d was detected using the phycoerythrin-labeled 34-5-8S antibody (BD Biosciences). Cells were analyzed by flow cytometry (FACSCalibur, BD Biosciences).

MCMV Infection, Cell Surface Staining, and FACS

70% confluent NIH3T3 cells were infected with MCMV-GFP (a virus containing GFP at an innocuous site (19)) at a multiplicity of infection of two. Twenty-four hours post infection (p.i.) the cells were detached with a non-enzymatic cell dissociation solution (Cellstripper, Cellgro) and resuspended in phosphate-buffered saline containing 5% fetal calf serum and 0.1% NaN_3. $F(ab')_2$ fragments were generated from monoclonal antibody mAb153.16 with the Immunopure IgG_1 $F(ab')_2$ kit (Pierce). Infected and uninfected cells were incubated with the $F(ab')_2$ followed by anti-mouse IgG-allophycocyanin. Dead cells were excluded by propidium iodide gating. Cells were analyzed with a FACSCalibur, and virus-infected cells were gated on GFP expression.

Bimolecular Fluorescence Complementation (BiFC)

NIH3T3 cells were transfected with 153-N-YFP and 153-C-YFP or 144-N-YFP and 144-C-YFP using the Amaxa nucleofector (solution R, program U30). Cells were then seeded on chambered coverslides and incubated for 48 h at 37 °C. A Leica TCS AOBS SP2 confocal microscope (Leica Microsystems) equipped with a 63 × 1.4 numerical aperture PL APO objective was used to examine live cells at room temperature for YFP fluorescence complementation. Leica TCS v2.1547 software was used to capture the images. After analysis the cells were detached with trypsin, and the YFP-positive cells were quantified by flow cytometry.

Immunoprecipitation and Western Blots

Transiently transfected and virus-infected cell lines were processed for immunoprecipitation and Western blotting as detailed in the supplemental "Experimental Procedures."

Expression and Purification of m153 in S2 Cells

The pMT-Bip-m153-His construct together with puromycin and blasticidin resistance-encoding plasmids (10:1:1 ratio by weight) were transfected into S2 cells using Fugene6 (Roche Applied Science) according to the manufacturer's protocol. 48 h after transfection the cells were transferred to selective medium containing 5 μg/ml puromycin (Sigma) and 5 μg/ml blasticidin (Calbiochem). Resistant cells were maintained in selective medium in shaker cultures (28 °C, 100 rpm). Expression of m153 was induced with 1 mM $CuSO_4$ at a cell density of 2×10^7/ml. m153 was purified on a nickel-nitrilotriacetic acid column (Qiagen) and then subjected to SEC (Shodex KW802.5 or Amersham Biosciences Superdex 75). The His tag was removed by thrombin cleavage at 37 °C for 2 h, and the protein was purified by anion exchange chromatography (Mono Q, Amersham Biosciences). For preparation of a selenomethionine (SeMet) derivative of m153, the m153/S2 cells were grown in Orbigen insect cell medium to 2×10^7 cells/ml. The cells were then washed in methionine-free medium (Orbigen) and starved in this medium for 6 h under normal growth conditions. Protein expression was induced by simultaneous addition of 1 mM $CuSO_4$ and 60 μg/ml SeMet (Sigma). The SeMet-labeled protein was purified as described for the native protein.

Crystallization, Structure Determination, and Refinement

Crystals of the SeMet derivative of m153 were grown in hanging drops at 18 °C over 25% polyethylene glycol 2000 MME, 0.1 M Tris-HCl, pH 8 (Solution 24, The PEGs Suite, Qiagen). Addition of 0.5% β-D-maltoside to the drops yielded crystals that diffracted to 2.3 Å. Diffraction data for SAD phasing were collected on a single crystal on beamline X29A at the National Synchrotron Light Source, Brookhaven, at a wavelength of 0.9791 Å and processed with HKL2000 (20). The automated SOLVE/RESOLVE scripts as incorporated in the AutoSol module of the PHENIX suite (21) were used with data truncated at 2.8 Å to obtain SAD phases followed by automated model building and docking to the m153 sequence. Ambiguously placed residues were rebuilt manually into the SAD-phased map in Coot as alanines (22). To extend the resolution to 2.4 Å a molecular replacement search was carried out in Phaser (23) with the partially built model yielding Z-scores of 11.0 and 23.7 for the rotation and translation functions, respectively, for one dimer in the asymmetric unit. Rigid body refinement specifying α1α2 and α3 as separate domains yielded a model with initial R and R_{free} of 36.9% and 38.6%, respectively. Refinement at 2.4 Å was continued in Refmac5 (24) with tight NCS restraints between chains A and B with further model building guided by $2F_o - F_c$ and $F_o - F_c$ maps generated in Coot. Although data were collected to 2.3 Å, data in the 2.38–2.3 shell were of insufficient quality and completeness. Therefore only data to 2.4 Å were used in refinement. Residues in the 231–237 loop, which had little or no electron density, were omitted from the NCS restraints. Optimal domains for TLS refinement were identified and input files for TLS refinement were generated using the TLSMD web server (25). TLS refinement using 10 TLS groups per chain decreased R_{free} from 29.9% to 28%. Finally, waters were added with CNS (26), and a final round of refinement was performed without NCS restraints. The final model has R_{cryst} = 23% and R_{free} = 27.9%, includes residues 2–230 and 238–277 of chain A and residues 5–277 of chain B and has 57 waters. The atomic coordinates and structure factors have been deposited in the Protein Data Bank (27)

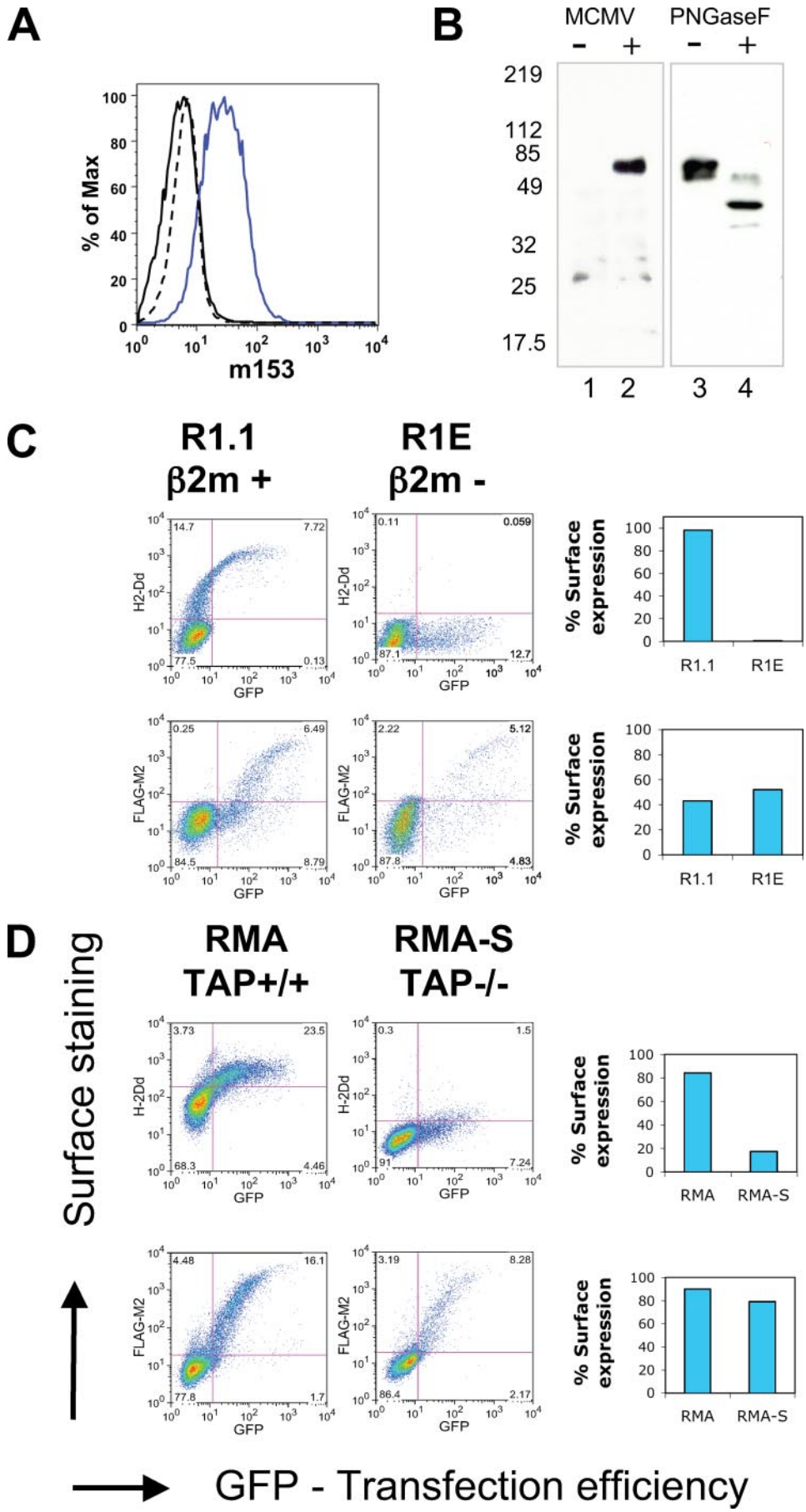

under accession number 2O5N. Buried surface area calculations were performed in CNS. Figures were generated using PyMOL, according to the manufacturer's manual (28).

Hinge angles were calculated using HINGE, a program written by Peter Sun. HINGE calculates an ellipsoid (defined by axes *a*, *b*, and *c*) for each indicated domain and reports the angle between the long axes of the adjacent domains as the hinge angle. HINGE is available at http://sis.niaid.nih.gov/programs/hinge.html.

Transient Expression of Wild-type and Mutant m153 in SF9 Cells

Alanine mutations were introduced simultaneously at four residues (Thr-128, Ser-131, Arg-225, and Ser-241) in the m153-N-YFP construct using the QuikChange Multi mutagenesis kit (Stratagene). Wild-type and mutated m153 (residues −22–382) genes were PCR-amplified from the m153-N-YFP and m153-N-YFP-mutant constructs using primers 5′CGTCA*CCCATG*-*G*CAATTCCCCTTCTCCTTCT-GCCGTTGGTTCTC and 5′ACT-TCG*CTCGAG*GGTGAGTCTCG-AATCGTTGATCGTCCTCTG. The PCR products were digested with NcoI and XhoI and inserted into the corresponding sites of the pIEx-4 SF9 expression vector (Novagen). 200 μg of m153-pIEx-4 or quadruple mutant-m153-pIEx-4 were transfected into 1×10^8 exponentially growing SF9 cells in 100 ml with 1 ml of Insect GeneJuice transfection reagent (Novagen). 72 h after transfection the cell supernatants were collected. Wild-type and quadruple mutant m153 were then purified on nickel-nitrilotriacetic acid and SEC columns as described for S2 insect cell expression.

Analytical Ultracentrifugation

Sedimentation velocity experiments were conducted with a ProteomeLab XLI ultracentrifuge (Beckman Coulter). 400-μl samples were loaded at concentrations of 0.3 mg/ml for m153 wild-type and 0.5

and 0.1 mg/ml for the m153 mutant and centrifuged at 50,000 rpm at 20 °C. Sedimentation data were acquired with the Rayleigh interference optical system at 1-min intervals, and data were analyzed using SEDFIT software (29).

RESULTS

m153 Is Expressed on the Surface of MCMV-infected Fibroblasts—The open reading frame of the *m153* gene predicts a type I transmembrane glycoprotein with a core molecular mass of 45 kDa. As a first step in the functional characterization of m153, we examined its expression in MCMV-infected fibroblasts. NIH3T3 cells, infected with MCMV at a multiplicity of infection of 2, expressed readily detectable levels of m153 at the cell surface 24 h p.i. as detected by the monoclonal antibody mAb153.16, specific for the extracellular domain of m153 (Fig. 1*A*). Uninfected cells did not stain with this antibody. By immunoprecipitation m153 was detected in lysates of infected cells as early as 3 and up to 48 h after infection with protein levels peaking at 24 h p.i. (data not shown).

Immunoprecipitation of cell lysates followed by SDS-PAGE and Western blot analysis of m153 revealed an unexpectedly high apparent molecular mass of 80 kDa, which was decreased to 45 kDa upon deglycosylation with peptide *N*-glycosidase F (Fig. 1*B*). Such heavy glycosylation is consistent with six predicted sites for asparaginyl-carbohydrate addition.

Cell Surface Expression of m153 Is Independent of β2m or TAP Expression—Because the MHC-I fold was predicted for all members of the MCMV m145 family (4), we next determined whether m153 shares the requirements of classic MHC-I molecules for β2m and peptide for stable expression. To investigate its requirement for β2m, we transfected N-terminally FLAG-tagged m153 (FLAG-m153) into a cell line deficient in β2m (R1E (30)) as well as its β2m-sufficient counterpart (R1.1). m153 surface expression was equivalent in both cell types indicating that m153 does not require β2m for stable surface expression (Fig. 1*C*).

To evaluate the requirement for bound peptide, we examined surface expression of m153 in RMA-S, a TAP-deficient cell line that fails to transfer peptides from the cytosol to the endoplasmic reticulum (31). MHC-Ia molecules expressed in such cells are unstable at the cell surface. We transfected RMA-S and RMA (TAP^+) cells with FLAG-m153 and evaluated surface expression of the viral protein in comparison to transfected H-$2D^d$, an MHC-Ia molecule (Fig. 1*D*). TAP deficiency had no effect on m153 surface expression, whereas expression of H-$2D^d$ was clearly reduced. We conclude that m153 does not require β2m or bound peptide for stable surface expression.

MHC-I Fold of m153—To elucidate the structure of m153 an SeMet derivative was prepared by biosynthetic labeling of the protein expressed in *Drosophila* S2 cells. SEC indicated that soluble m153 was a dimer (supplemental Fig. S1). Diffraction data from a single crystal were collected, the structure was solved by SAD phasing, and the model was refined at 2.4-Å resolution to final R_{cryst} and R_{free} of 23 and 27.9, respectively (Table 1). There is a single dimer in the asymmetric unit with chains designated A and B. We observed continuous electron density for residues 2–230 and 238–277 of chain A and residues 5–277 of chain B. No electron density was observed for the C-terminal residues 278–314 of either chain, and these were omitted from the model. The average *B*-factor was 42 $Å^2$ for chain A and 32 $Å^2$ for chain B. We selected chain B to describe the structural features of the monomer as they relate to the MHC-I fold, because it is more complete and has lower *B*-factor values.

TABLE 1
Data collection, refinement, and validation statistics

Data collection	
Space group	$P2_1$
Unit cell dimensions	
a, b, c	61.7, 78.2, 62,7
α, β, γ	90, 90.4, 90.0
Molecules per asymmetric unit	2
Resolution (Å)	2.3
Total observations	335,101
Unique reflections	26,191
Completeness (%)[a]	97.5 (94.2)
$I/\sigma I$[a]	9.7 (2.0)
R_{sym}[a,b]	0.081 (0.44)
Refinement	
Resolution range	62.75–2.4
Reflections	
Working set	23,443
Test set	1183
R_{cryst} (%)[c]	23.0
R_{free} (%)[c]	27.9
Number of non-H protein atoms	4,393
Number of water molecules	57
Carbohydrate chains	3
r.m.s. deviations from ideality	
Bond lengths (Å)	0.01
Bond angles (°)	1.318
Average *B* values ($Å^2$)	A, B
Main chain	42.2, 32.2
Side chain	42.5, 32.7
Whole chain	42.4, 32.4
Overall	37.6
Model validation: Ramachandran plot statistics (Procheck) (%)	
Most favored	87.8
Allowed	12.2
Generous	0
Disallowed	0

[a] Values in parentheses are statistics for the highest resolution shell used in refinement (2.48-2.38 Å).
[b] $R_{sym}(I) = \Sigma|I_j - \langle I\rangle|/\Sigma I_j$, where I_j is the intensity of the *j*th observation of a reflection and $\langle I\rangle$ is the mean intensity from multiple measurements of that reflection.
[c] $R_{cryst} = \Sigma||F_o| - |F_c||/\Sigma|F_o|$, where F_o and F_c are the observed and calculated structure factor amplitudes, respectively. R_{free} is as for R_{cryst} but calculated for a randomly selected 5.0% of reflections not included in the refinement. Procheck was used for model validation (49).

The structure of m153 (Fig. 2) reveals basic structural elements of the MHC-I fold. The m153 α1α2 domain consists of a unit in which the α1 helix and a discontinuous α2 helix rest atop a platform of seven β-strands. Three of the strands derive from

FIGURE 1. **m153 expression at the surface of MCMV-infected, β2m-deficient, and TAP-deficient cells.** *A*, MCMV-infected NIH3T3 cells were surface-stained for m153 expression at 24 h post infection (p.i.). *Blue*, infected cells plus mAb153.16; *black*, infected cells plus control antibody; and *dashed line*, uninfected cells plus mAb153.16. *B*, immunoprecipitation and Western blot analysis of m153 from uninfected (*lane 1*) and MCMV-infected (*lane 2*) NIH3T3 cell lysates at 24 h p.i. Immunoprecipitation of m153 from transfected NIH3T3 cells (immunoprecipitation, mAb153.16; Western blot, anti-m153 rabbit serum). Samples were mock treated (*lane 3*) or treated with peptide *N*-glycosidase F (*lane 4*) before SDS-PAGE and Western blot. *C*, R1.1 (β2m^+) and R1E (β2m^-) or *D*, RMA (TAP^+) and RMA-S (TAP^-) cells were transfected with FLAG-m153-pIRES-GFP or H-$2D^d$-pIRES-GFP as a control. 18 h post transfection surface levels of m153 and H-$2D^d$ were determined as described under "Experimental Procedures." The number of GFP-positive cells indicates transfection efficiency. The percentage surface expression is shown in the *bar graphs* on the *right* (percentage of GFP^+ cells that stain for either FLAG-M2 or H-$2D^d$).

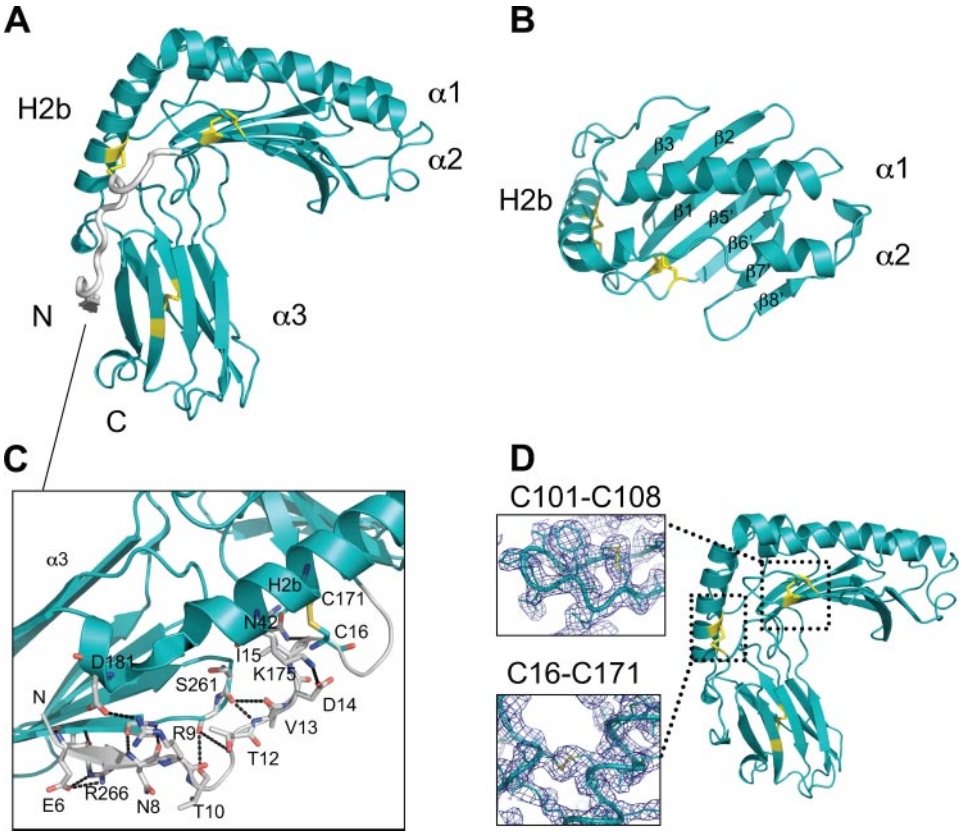

FIGURE 2. **Conserved and unique features of the m153 monomer.** *A*, side view of m153 chain B. The α1, α2, and H2b helices, the α3 domain, N and C termini are labeled, and the disulfide bonds are in *yellow*. N-terminal residues 2–20 are *gray*. *B*, top view of the seven β-strand platform and α1α2 helixes of m153. *C*, extended N terminus of m153 showing extensive interactions between the N terminus (*gray*) and H2b helix, loops in the α1α2 domain and the G strand of the α3 domain (*cyan*). Hydrogen bonds are in *black*. *D*, side view of m153 monomer. Two unique disulfide bonds link the N-terminal fragment to the H2b helix (*C16-C171*) and the β5′ platform strand to the loop connecting the β5′ and β6′ strands (*C101-C108*). Electron density around the unique disulfides is contoured at 1.25 σ. The conserved disulfide bond (Cys-203–255) is located in the Ig-like α3 domain.

the α1 domain and four from α2. The fourth β-strand of the α1 domain, commonly found in MHC-Ia and -Ib molecules, is not observed in m153. Unlike either MHC-Ia or -Ib molecules the C-terminal end of the α2-helix extends downward into a third helix (designated H2b) that connects the α1α2 domain with the Ig-like α3 domain (Fig. 2*A*).

Several structural features of the m153 monomer differ substantially from classic MHC-I molecules. Most striking is the N terminus, extended by 20 residues, which starts adjacent to the G strand of the α3 domain, forming a short β strand. From there it extends upward alongside the H2b helix and continues as the first strand of the platform beginning at residue 21 (Fig. 2*A*). This feature is absent in all MHC-I molecules described thus far and differs substantially from m157, whose extended N terminus forms instead a third, short helix adjacent to the α2 helix (Fig. 3, *A* and *C*). A unique disulfide between Cys-16 and Cys-171 anchors the extended N terminus of m153 to the H2b helix (Fig. 2*D*). In addition several hydrogen bonds link the extended N-terminal strand (residues 6–15) and the loop between platform strands β2 and β3. Other hydrogen bonds link the extended N terminus to the H2b helix and the α3 F-G loop and serve to further stabilize the structure (Fig. 2*C*). The α1 and α2 helices are shorter than those observed in MHC-Ia proteins and are closely juxtaposed above the β sheet floor. Close interactions between these helices preclude the binding of peptide or other ligand (Fig. 2*B*), in agreement with cellular expression studies indicating that m153 does not depend on bound peptide for stability (Fig. 1*D*). The platform is stabilized by a second unusual disulfide (Cys-101 to Cys-108), which connects strands β5′ and β6′ of the floor (Fig. 2*D*). A similar bond is seen in m157 (Cys-103 to Cys-112), but MHC-Ia molecules preserve a disulfide bond in the same region, which links β-strand 5 of the platform to the α2 helix (Cys-101 to Cys-164) (32). The presence of the unusual disulfide bonds in m153 was confirmed by mass spectrometry (supplemental Figs. S3 and S4).

The α3 domain of m153 has a C2-type Ig-fold, which is characterized by a more compact domain and shorter intercysteine spacing than the C1 or V-type fold (33). The A, B, and E strands make up one sheet of the domain, and the C, C′, F, and G strands make up the opposite sheet (Fig. 2*A*). The canonical Ig-domain disulfide bond (Cys-203 to Cys-255) connects strands B and F. Searches against the DALI data base (34) identified m144, also with a C2-type Ig-fold, and CD1d as proteins with α3 domains that are structurally most closely related to m153. The difference between the strand dispositions in the α3 domains of m153 and m157 is indicated by the relatively high r.m.s.d. of 2.3 Å for the superposition of 67 Cα atoms. The α3 domain of m153 has longer β-strands that exhibit the characteristic β-sandwich twist, whereas the m157 α3 domain has strands that are shorter and form flatter sheets (Fig. 3*C*). The terminal residues that were modeled in both structures adopt different conformations, in m153 they form a short α-helix, whereas in m157 the C-terminal strand forms a circular loop that contacts both sheets of the α3 domain (18).

In Fig. 3 we compare the α1α2 domain of m153 chain B to that of m157, H-2K^b (35), rat FcRn (36), and the NKG2D ligand Rae-1β (37). The α1 and H2b helices of m153 and m157 are in equivalent positions, whereas their α2 helices differ. The N-terminal end of the m157 α2 helix was not modeled due to lack of electron density (18). The m153 α2 helix starts with two full turns (residues 140–146), followed by an extended region that stretches along the platform ending in two turns of helix before bending sharply downward to continue as the H2b helix.

The maximal distance between the α1 and α2 helices of m153 is 8.1 Å compared with 16.8 Å in H-2K^b (Fig. 3*A*). Surface representations of the α1α2 domains of m153 and H-2K^b (Fig.

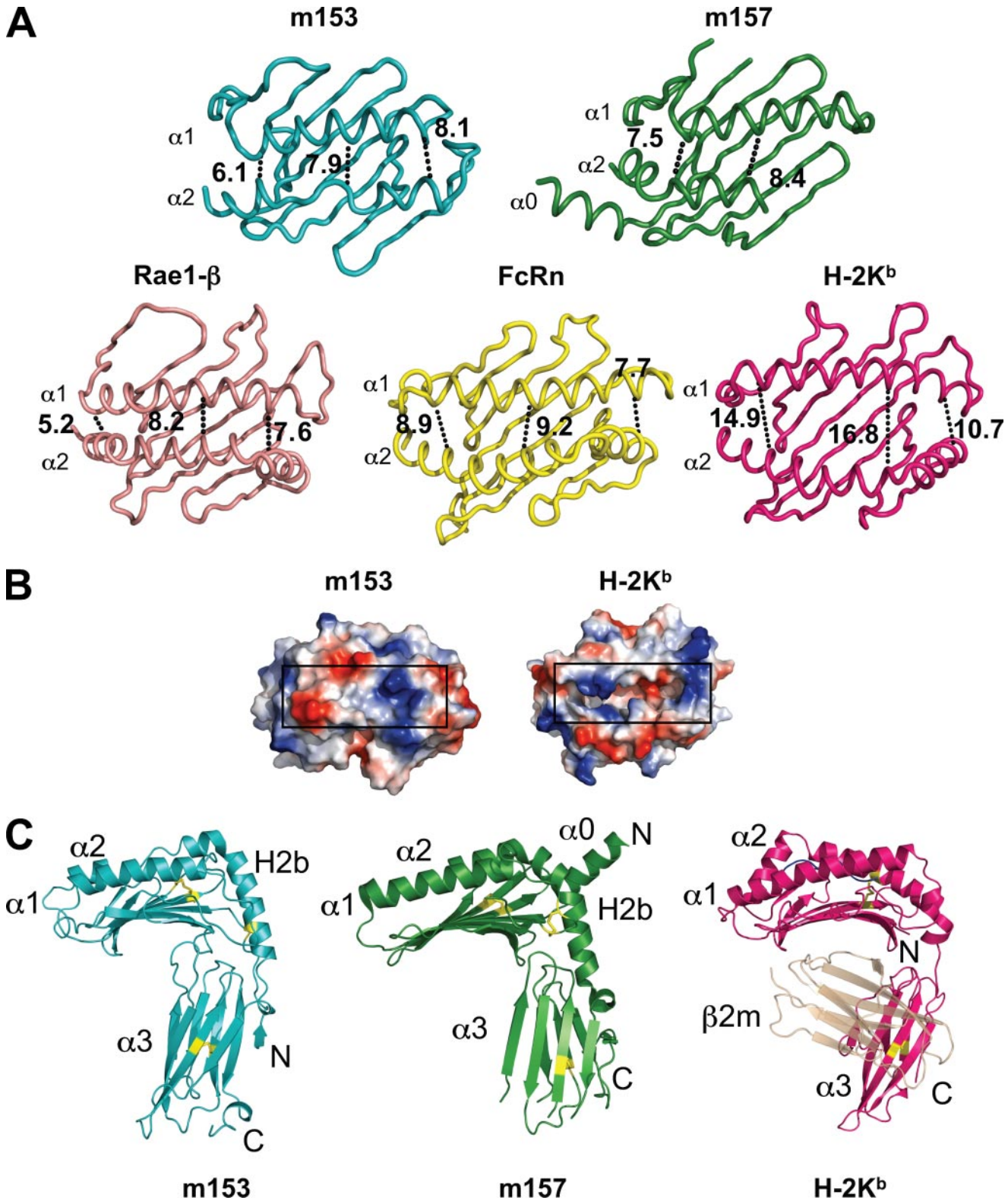

FIGURE 3. **Comparison of m153 with m157, H-2K^b, Rae-1β, and rat neonatal FcR.** *A*, ribbon diagrams of the platform domains of m153, m157, Rae1β, FcRn, and H-2K^b. The width of the groove of each molecule is indicated in angstroms and was measured at both ends and in the middle at comparable residues of the α-helices. *B*, surface representation of the peptide-binding domain of H-2K^b (groove shown without any peptide) and the corresponding region of m153. *Black rectangles* indicate the groove. *C*, comparison of m153 chain B with m157 and H-2K^b. The α1α2 and H2b-helices, α3-domain, and N and C termini are labeled. PDB accession codes are: 2NYK, 2VAA, 1JFM, and 3FRU.

3*B*) illustrate the lack of a peptide-binding groove in m153. The groove region of m153 is comparable to that of Rae-1β and FcRn, two molecules that also do not bind peptide. The maximal distance between Cα atoms of the α1 and α2 helices of Rae-1β and FcRn are 8.2 Å and 9.2 Å, respectively. The α1 helices of m153, Rae-1β, and FcRn have a similar arrangement on the platform, but the m153

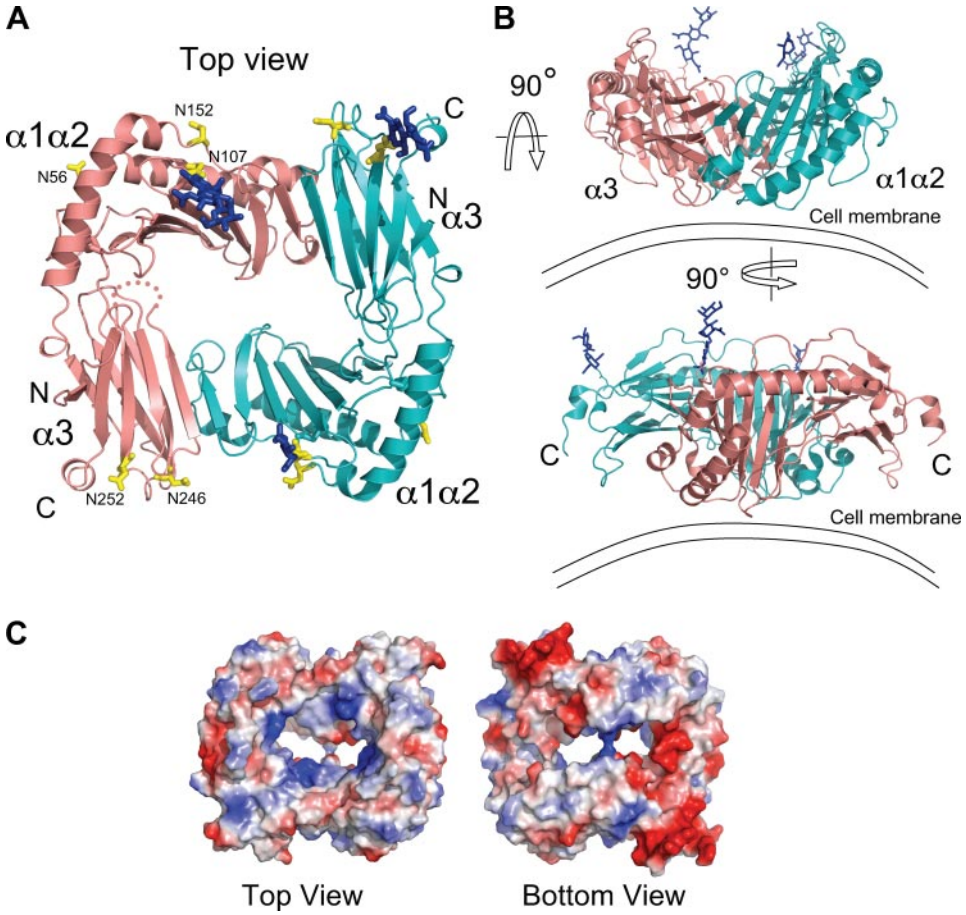

FIGURE 4. **Overall structure of the m153 dimer.** *A*, ribbon diagram of the m153 dimer as viewed from the *top*. Chain A, *salmon*; chain B, *cyan*. The α1α2 helices, the α3 Ig-like domains, and N and C termini are labeled. The *dashed line* in chain A indicates a disordered loop. *Blue sticks*, carbohydrates observed in the crystal structure; *yellow sticks*, *N*-linked glycosylation sites confirmed by mass spectrometry. *B*, two 90° rotations reveal different side views of the m153 dimer, and its proposed orientation on the cell membrane. *C*, top and bottom views of the electrostatic surface representation of the m153 dimer (*red*, acidic; *blue*, basic).

helix is shorter. The m153 platform has seven strands compared with the eight found in classic MHC-I proteins (Fig. 3*A*).

The hinge angle between α1α2 and α3 of m153 chain B is 76°, which is within the range of the MHC-I molecules H-2K^b, CD1d, and T22 (71–74°) but is smaller than that of m157 (81°), MICA (116°), and m144 (99°) (supplemental Table S1). The m153 α3 domain makes extensive contacts with the H2b helix, with the loop connecting strands β2 and β3 of the platform as well as with the loop connecting β3 and α1. The buried surface area between α1α2 and α3 of m153 is 1777 Å^2, which is considerably larger than the analogous interfaces in m157 (1265 Å^2) and H-2K^b (455 Å^2).

m153 Dimer—SEC of the insect cell-expressed extracellular portion of m153 indicated that the molecule formed a stable non-covalent homodimer (supplemental Fig. S1), an observation confirmed by equilibrium and velocity sedimentation (data not shown). The crystal structure reveals the details of the mode of dimerization. Two MHC-I-like chains of m153 are organized in a head-to-tail arrangement forming a compact dimer (Fig. 4*A*). The two chains are almost identical (r.m.s.d. of 0.624 Å for superposition over 268 Cα atoms). The interaction of the platform domain of one subunit with the α3 domain of the other imparts a coronal shape forming a central cavity with a volume of ~9500 Å^3. The conical cavity measures 46 Å × 35 Å at the top narrowing down to 22 Å × 18 Å. It is closed off at the bottom where the Lys-115 side chains of each subunit are only 4 Å apart. We propose an orientation of the m153 dimer with respect to the plasma membrane shown in Fig. 4*B*. The subunits lie with their long axes parallel to the membrane and with the α1 helices closest to the membrane. In this orientation the C termini of both chains point toward the membrane (Fig. 4*B*, *lower*). The 37 C-terminal residues for which no electron density was observed in either chain may form a flexible stalk connecting the ectodomain to the transmembrane region. m153 conserves only two of the 31 β2m-contacting residues present in H-2K^b. It is evident from the dimer orientation of m153 that association with β2m would be sterically hindered, an observation consistent with the β2m independence of m153 expression (Fig. 1*C*).

Three sugar moieties were modeled in the m153 structure (at Asn-107 in chains A and B and Asn-252 in chain B). These all point upward from the dimer away from the cell surface. Mass spectrometry indicated glycosylation at five of the six predicted *N*-linked carbohydrate addition sites (data not shown). These sites occur in both α1α2 and α3 and are distributed around the periphery of the m153 dimer, with none in the central cavity or at the proposed membrane proximal face of the molecule (Fig. 4*A*). The electrostatic surface of the m153 dimer reveals four nearly symmetrical basic patches inside the central cavity, and two highly acidic regions on the bottom surface that are formed by the loop that connects the A and B strands of the α3 domain and the C-terminal α-helical fragment (Fig. 4*C*).

The m153 dimer interface is formed by parallel β-strand interactions between the platform (β8′ strand) of one subunit and the α3 domain (C′ strand) of the second subunit (Fig. 5*A*), resulting in two extended, twisted β-sheets of 12 strands each that form the core of the dimer. The two interfaces are not perfectly symmetrical as 21 residues of chain A and 22 residues of chain B are involved in dimerization. There are 16 hydrogen bonds at the interface, most of which represent backbone interactions (Fig. 5*B*). In addition there are 114 non-bonded contacts. The area buried at the dimer interface is 1088 Å^2, which is larger than that observed in HLA-G (676 Å^2), which forms a disulfide-linked MHC-Ib dimer (Fig. 5*C*). The shape complementarity index of the dimer was calculated as 0.72, which is higher than that of most antibody-antigen interfaces (0.62–0.68), consistent with the stability of the homodimer (shape

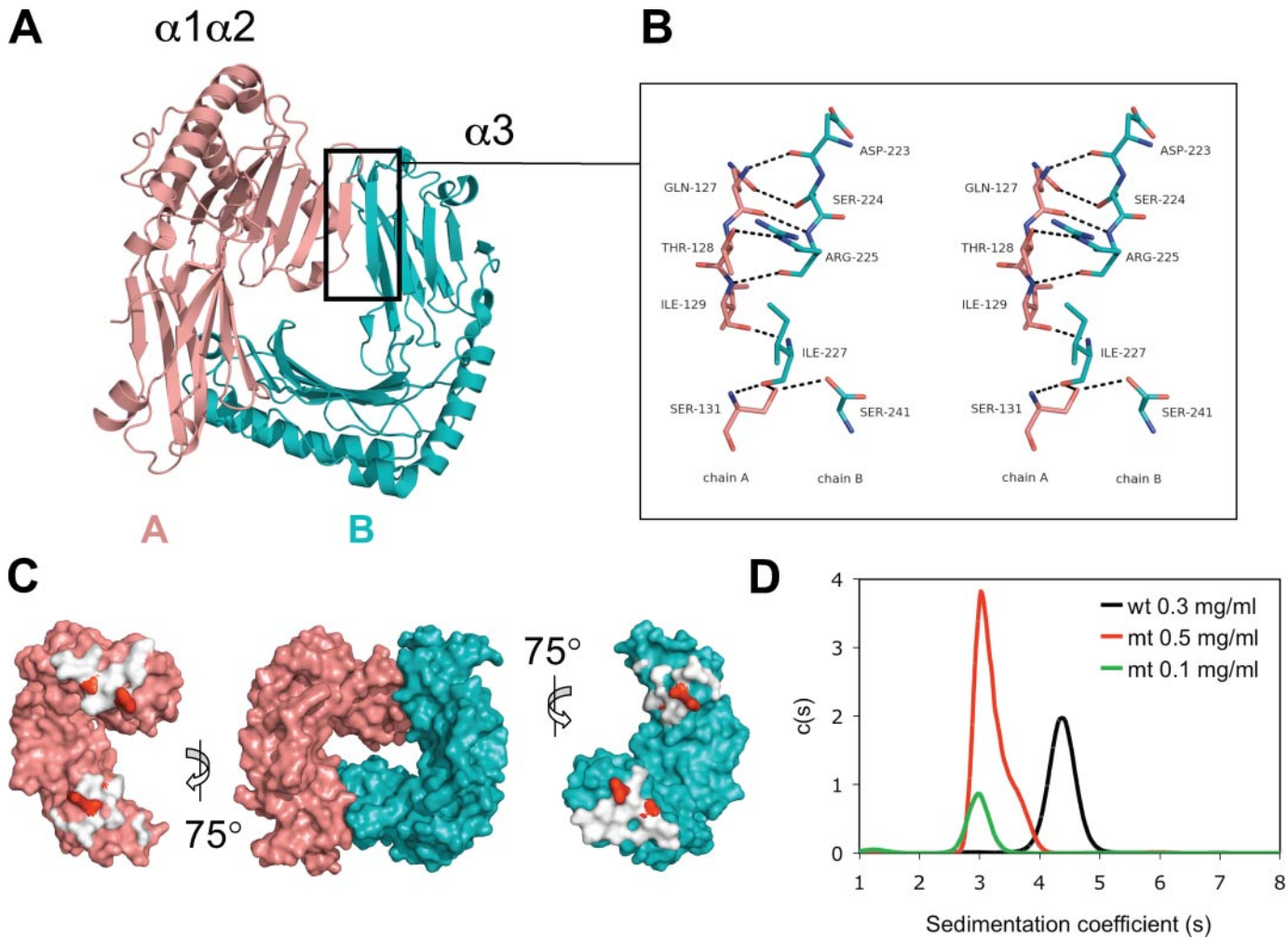

FIGURE 5. **Dimer interface of m153.** *A*, chain A-platform/Chain B-α3 interface indicated by the *boxed region*. *B*, stereo view of the parallel β strand interactions between the β8′ strand of chain A (*salmon*) and the G strand of chain B (*cyan*). The nine hydrogen bonds are shown as *black dashes*. Oxygen, *red*; nitrogen, *blue*. *C*, molecular surface representation of m153 dimer (*center*). At the left and right the two chains were rotated 75° out of the plane of the paper (or screen) to display the buried interaction surfaces (*white*). The positions of the interface residues that were mutated to alanine (Thr-128, Ser-131, Arg-225, and Ser-241) are shown in *red*. *D*, mutations at the interface destabilize the m153 dimer. Sedimentation coefficients of wild-type m153 (*black*, 0.3 mg/ml) and quadruple mutant m153 (T128A,S131A,R225A,S241A; *red*, 0.5 mg/ml; *green*, 0.1 mg/ml) as determined by sedimentation velocity ultracentrifugation.

complementarity index = 1 represents a perfect fit (38)). To confirm the observed interface we tested the effects of mutating four interface residues Thr-128, Ser-131, Arg-225, and Ser-241, all of which form side-chain/side-chain hydrogen bonds, to alanine (Fig. 5*C*). Wild-type m153 and a mutant containing these four alanine mutations were expressed and analyzed by ultracentrifugation and SEC. The mutant protein had a smaller sedimentation coefficient indicating disruption of the dimer (Fig. 5*D*). SEC confirmed the smaller size of mutant m153 (supplemental Fig. S5). Thus the four mutations destabilized the m153 dimer and confirm the mode of dimerization visualized in the structure.

Full-length m153 Is Dimeric in Mammalian Cells—To exclude the possibility that dimerization is a result of the engineering of soluble m153, we used two approaches to examine m153 in mammalian cells. In BiFC (39) experiments we fused full-length m153 to either N- or C-terminal segments of YFP. Although transfectants of either construct alone did not show fluorescence, co-transfection of m153-N-YFP and m153-C-YFP resulted in the complementation of YFP fluorescence in transfected cells (Fig. 6*A* and supplemental Fig. S2), indicating that m153 does form dimers. Cells transfected with YFP fusion constructs of m144, a monomeric MHC-Iv protein, showed less than 1% YFP-positive cells. In a second approach we co-transfected N-terminal FLAG- and HA-tagged m153 in NIH3T3 cells. Successful immunoprecipitation of m153 with anti-FLAG antibodies and Western blot detection with anti-HA antibodies confirmed that m153 dimerizes in transfected fibroblasts (Fig. 6*B*). Together these results provide strong evidence that m153 is a dimer when expressed as the full-length protein in mammalian cells.

Comparison of m153 to the m145 Family—m153 is related by sequence to proteins of the mouse and rat CMV 145 families but has no direct homolog in the rat virus (3, 40). The m153 protein is most closely related to m152 (28% identity), a known regulator of MHC-I and NKG2D ligands in MCMV-infected cells (14, 16). Fig. 7 shows a sequence alignment of the m145 family highlighting shared structural features. Based on comparison of m153 and m157, we suggest that the core of the viral MHC-I-like fold of the m145 family is composed of the α1α2 domain, the extended H2b helix, and an Ig-like α3 domain. The number of platform strands, the length of α2 on top of the

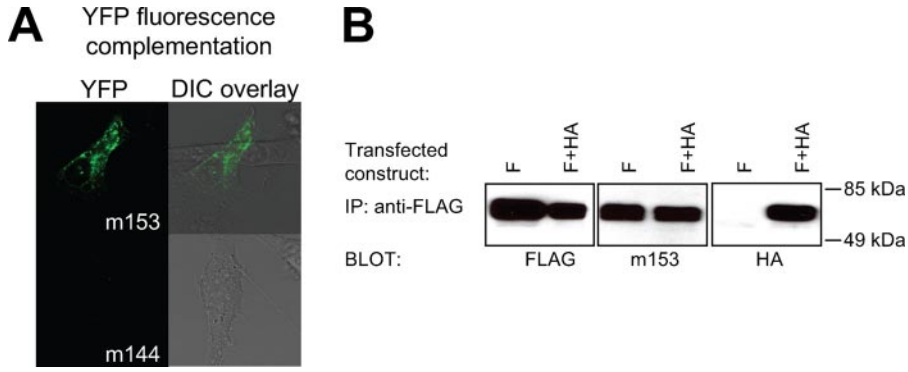

FIGURE 6. **m153 forms a homodimer in mammalian cells.** *A*, BiFC analysis. m153 constructs, fused to the N- or C-terminal portions of YFP, were cotransfected in NIH3T3 cells, and the live cells were examined by confocal microscopy for fluorescence complementation after 48 h. As a negative control YFP fusion constructs of MCMV m144 were co-transfected. *Left*, YFP channel; *right*, overlay of the YFP on the differential interference contrast (*DIC*) channel. Quantification of the number of YFP-positive cells is shown in supplemental Fig. S2. *B*, co-immunoprecipitation of differentially tagged m153. FLAG-m153 (*F*) or F plus HA-m153 (*F+HA*) constructs were transfected in NIH3T3 cells. 24-h post transfection post nuclear cell lysates were immunoprecipitated with anti-FLAG antibodies and detected on a Western blot with anti-FLAG (*left*), anti-m153 rabbit antibodies (*middle*), or HA-specific antibodies (*right*).

platform, and the position of some disulfide bonds may vary. A crucial stabilizing interaction for this MHC-I-like fold is that between Glu-70 (α1 helix), Arg-166, and Trp-167 (H2b helix). Apart from a cysteine in the α3 domain, these three residues are the only amino acids that are conserved throughout the mouse and rat 145 families, emphasizing the importance of this salt bridge. Within the m145 family stretches of similarities are found in α helix and β sheet regions, whereas loop regions and the α3 domain show less conservation. The m153 residues involved in dimerization are not conserved in the rest of the family consistent with our observation that m151 and m152 do not dimerize in solution.[5] Thus dimerization may be unique to m153. Five family members contain cysteines that align with those of the unusual m153 Cys-16 to Cys-171 disulfide. The Cys-101 to Cys-108 and Cys-203 to Cys-255 disulfides are also conserved among some of the family members. The limited sequence similarity of the N- and C-terminal regions of the extracellular domains of the m145 family members likely indicates a structural divergence in these parts of these molecules.

DISCUSSION

MHC-I molecules play a crucial role in the protection of the host against virus infection. Not only are MHC-I molecules essential for the detection of infection and priming of the cytotoxic $CD8^+$ T-cell response, but their presence on the cell surface protects healthy cells from attack by NK cells. Viral molecules with an MHC-I-like structure are likely to be excellent decoys for inhibitory NK receptors and may be able to interact with numerous molecules involved in the immune response. It is therefore not surprising that herpesviruses have incorporated MHC-I-like molecules in their arsenal of immunoevasins. Human, mouse, and rat CMV encode MHC-I-like molecules that exhibit different levels of similarity to MHC-Ia molecules (3, 40). HCMV encodes the MHC-I homolog UL18, which binds both β2m and peptide and engages the inhibitory receptor LIR-1 (41). It also encodes UL142, which functions to inhibit NK cell lysis, has less sequence similarity to MHC-I, and is predicted to consist of only the MHC-I α1α2 domain (42). MCMV encodes proteins like m144 that can associate with β2m, and others like m153 and m157, members of the m145 family, that are expressed without β2m. It is likely that several host genes have been captured by viruses during the course of co-evolution (43). In the case of the MHC-I viral homologs it is probable that the closely related MHC-I genes like *m144* and *r144* were originally acquired from the host and that the distantly related *m145* and *r145* families arose via gene duplication and expansion of the *144* gene shaped by the selective pressures of the host immune response.

The crystal structure of MCMV m153 provides an example of the versatility of the MHC-I fold and is the first report of an obligate non-covalent dimer composed of two MHC-I-like chains. Together with the recently reported m157 structure, it highlights both the conserved and divergent features of the m145 family. The m153 monomer retains the core MHC-I characteristics, a β-sheet platform that supports two α-helices and an Ig-like α3 domain, but it exploits several structural adaptations to yield a stable molecule in the absence of peptide and β2m. Three main features combine to stabilize the m153 monomer: 1) the closely spaced α1 and α2 helices on the platform do not form a groove and alleviate the need for peptide binding; 2) the extended H2b helix bridges the α1α2 domain to the α3 domain; and 3) numerous interdomain contacts and two unique disulfide bonds (Cys-16 to Cys-171 and Cys-101 to Cys-108) stabilize the structure. Some of these features are shared among the other members of the m145 family. Whereas m157 is linked to the cell membrane via a glycophosphatidylinositol moiety and functions as a monomer (2), m153 has a *bona fide* transmembrane region and a large (47-amino acid) intracellular domain. We have shown that m153 is a stable dimer when expressed in mammalian cells, and the crystal structure of the soluble ectodomain reveals the mode of dimerization.

Dimerization is unusual for MHC-I molecules. Although dimers of some classic MHC-I molecules have been reported, *i.e.* HLA-B27 (44) and HLA-G (45), these are disulfide-linked and their physiological relevance remains unclear. A non-disulfide linked dimer has been observed in crystals of the rat FcRn. Unlike m153, the two MHC-I molecules of the FcRn interact via their α3 and β2m domains, utilizing extensive protein-protein and protein carbohydrate interactions at the interface (36). In the m157 crystal, a dimer of the same orientation as m153 is formed with one of the symmetry-related molecules. In m157 this dimer interface is formed by anti-parallel β strand interactions between the β6 strand of the platform and the D strand of the α3 domain. Thus the same chain orientation but an opposite sheet of the α3 domain (strands A, B, E, and D) is utilized in the observed crystal packing.

[5] J. Mans, K. Natarajan, A. Balbo, P. Schuck, C. T. Tiemessen, and D. H. Margulies, unpublished observation.

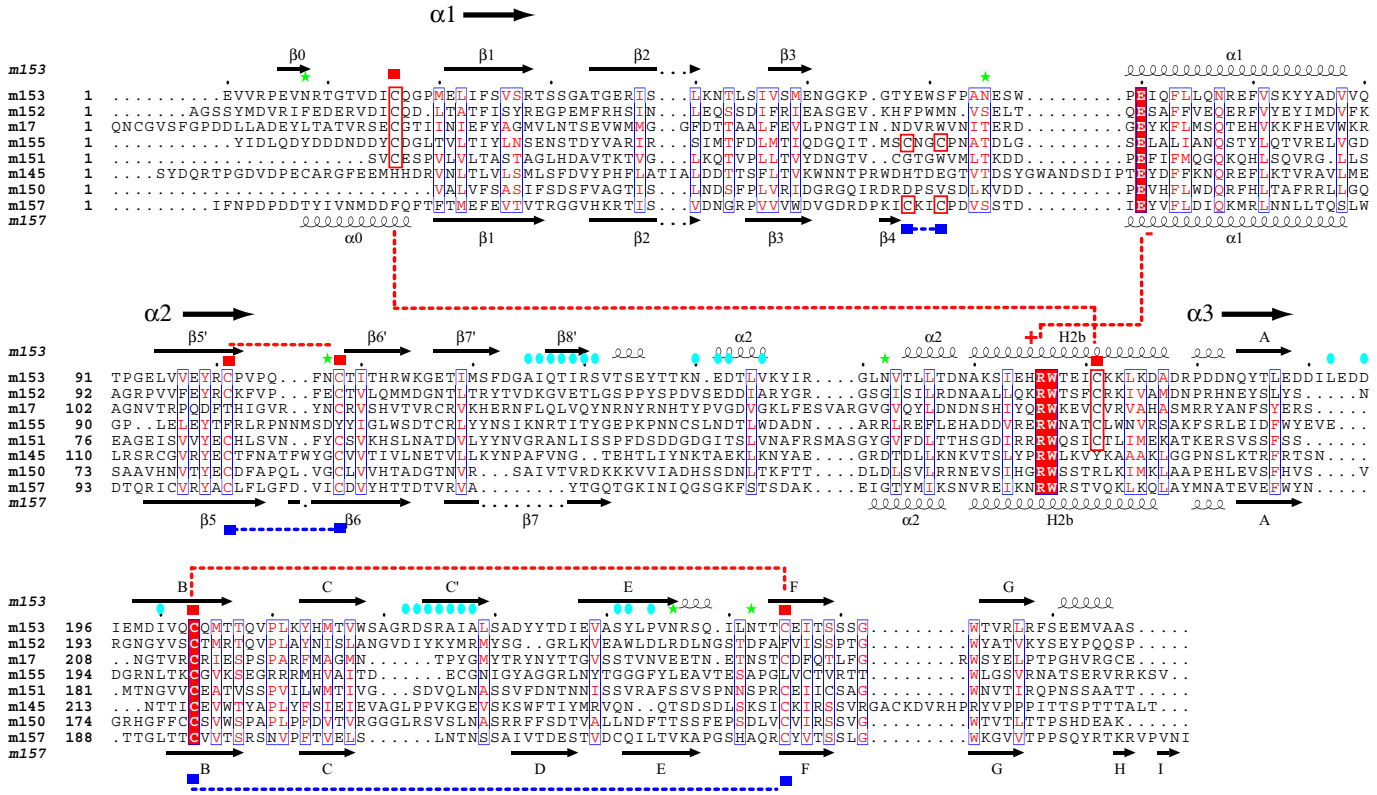

FIGURE 7. **Amino acid sequence alignment of the m145 family.** The predicted extracellular domains of all m145 family members (Refseq: NC_004065 (3)) were aligned using ClustalW (47) and optimized based on m153 and m157 structure. Secondary structure elements of m153 are shown above and those of m157 shown below the alignment. Cysteines involved in disulfide bonds are indicated by *red* (m153) and *blue* (m157) *squares*, and the respective pairs are indicated. Cysteines that are not conserved throughout the family, but are predicted to form disulfide bonds are *boxed in red*. Residues involved in a salt bridge (Glu-70 and Arg-166) are also indicated. *N*-Linked glycosylation sites are indicated by *green stars*. The residues involved in m153 dimer interface contacts are indicated by *blue ovals*. The figure was generated with ESPRIPT (48).

To gain insight into possible ligand binding sites on m153 we have examined regions corresponding to known interaction sites on murine MHC-I like molecules. These include the CD8$\alpha\alpha$ binding site (α3 domain residues 220–228 and residues of the α1α2 domain platform), the Ly49A NK receptor binding site ("site 2," including residues from the α3 domain, the α1α2 domain platform, and key residues of β2m), and the region of the FcRn-Fc interaction site (N-terminal portions of the α2 domain and of β2m) (7). The compact nature of the m153 dimer, its lack of β2m association, and the regions that are masked by dimerization make it unlikely that any of the above mentioned sites are available for ligand binding.

Because m153 is clearly related to other immunoevasins by both amino acid sequence and structure, it may be expected also to function to subvert the host immune response. Several features strongly indicate that m153 has a significant role in the viral life cycle: 1) Several regions of the m153 sequence are conserved among related molecules with known immunoregulatory function. m152 and m155 conserve the Cys-16 to Cys-171 disulfide, and m152 and m145, as well as m157, conserve the β5′-β6′ Cys-101 to Cys-108 disulfide. 2) This is a readily expressed viral glycoprotein, easily detected both intracellularly and at the cell surface in MCMV-infected fibroblasts. 3) Heteroduplex mobility assay and DNA sequence analysis have been used to examine the levels of sequence variation of a number of MCMV genes of isolates from wild mice and laboratory strains. The MHC-Iv immunoevasins m144, m155, and m157 have significant variation, whereas m152 is highly conserved (17, 46). m153, like m152, is highly conserved among many strains showing little variation by both heteroduplex mobility assay and sequencing.[6] Such conservation implies not only a role in viral survival but suggests that m153, like m152, may interact with an invariant site on a host molecule (46). Further experiments will explore the identification of cellular and molecular ligands and test the contribution of m153 to acute and chronic stages of viral infection.

Acknowledgments—We thank Barbara Newman and Rose Mage for production of rabbit antiserum, members of the Molecular Biology Section, Laboratory of Immunology, NIAID, NIH for their help, and Sam Xiao and Jack Bennink for comments on the manuscript. Support for beamline X29 of the National Synchrotron Light Source comes principally from the Offices of Biological and Environmental Research and of Basic Energy Sciences of the U.S. Department of Energy and from the National Center for Research Resources of the National Institutes of Health.

REFERENCES

1. Tortorella, D., Gewurz, B. E., Furman, M. H., Schust, D. J., and Ploegh, H. L. (2000) *Annu. Rev. Immunol.* **18,** 861–926
2. Arase, H., Mocarski, E. S., Campbell, A. E., Hill, A. B., and Lanier, L. L. (2002) *Science* **296,** 1323–1326

[6] L. Smith and A. Redwood, personal communication, University of Western Australia, 2007.

3. Rawlinson, W. D., Farrell, H. E., and Barrell, B. G. (1996) *J. Virol.* **70,** 8833–8849
4. Smith, H. R., Heusel, J. W., Mehta, I. K., Kim, S., Dorner, B. G., Naidenko, O. V., Iizuka, K., Furukawa, H., Beckman, D. L., Pingel, J. T., Scalzo, A. A., Fremont, D. H., and Yokoyama, W. M. (2002) *Proc. Natl. Acad. Sci. U. S. A.* **99,** 8826–8831
5. Bjorkman, P. J., and Parham, P. (1990) *Annu. Rev. Biochem.* **59,** 253–288
6. Natarajan, K., Li, H., Mariuzza, R. A., and Margulies, D. H. (1999) *Rev. Immunogenet.* **1,** 32–46
7. Margulies, D. H., Natarajan, K., Rossjohn, J., and McCluskey, J. (2007) in *Fundamental Immunology* (Paul, W. E., ed) Lippincott, Williams, and Wilkins, Philadelphia, in press
8. Beck, S., and Barrell, B. G. (1988) *Nature* **331,** 269–272
9. Farrell, H. E., Vally, H., Lynch, D. M., Fleming, P., Shellam, G. R., Scalzo, A. A., and Davis-Poynter, N. J. (1997) *Nature* **386,** 510–514
10. Chapman, T. L., and Bjorkman, P. J. (1998) *J. Virol.* **72,** 460–466
11. Natarajan, K., Hicks, A., Mans, J., Robinson, H., Guan, R., Mariuzza, R. A., and Margulies, D. H. (2006) *J. Mol. Biol.* **358,** 157–171
12. Hasan, M., Krmpotic, A., Ruzsics, Z., Bubic, I., Lenac, T., Halenius, A., Loewendorf, A., Messerle, M., Hengel, H., Jonjic, S., and Koszinowski, U. H. (2005) *J. Virol.* **79,** 2920–2930
13. Krmpotic, A., Hasan, M., Loewendorf, A., Saulig, T., Halenius, A., Lenac, T., Polic, B., Bubic, I., Kriegeskorte, A., Pernjak-Pugel, E., Messerle, M., Hengel, H., Busch, D. H., Koszinowski, U. H., and Jonjic, S. (2005) *J. Exp. Med.* **201,** 211–220
14. Lodoen, M., Ogasawara, K., Hamerman, J. A., Arase, H., Houchins, J. P., Mocarski, E. S., and Lanier, L. L. (2003) *J. Exp. Med.* **197,** 1245–1253
15. Lodoen, M. B., Abenes, G., Umamoto, S., Houchins, J. P., Liu, F., and Lanier, L. L. (2004) *J. Exp. Med.* **200,** 1075–1081
16. Ziegler, H., Thale, R., Lucin, P., Muranyi, W., Flohr, T., Hengel, H., Farrell, H., Rawlinson, W., and Koszinowski, U. H. (1997) *Immunity* **6,** 57–66
17. Voigt, V., Forbes, C. A., Tonkin, J. N., Degli-Esposti, M. A., Smith, H. R., Yokoyama, W. M., and Scalzo, A. A. (2003) *Proc. Natl. Acad. Sci. U. S. A.* **100,** 13483–13488
18. Adams, E. J., Juo, Z. S., Venook, R. T., Boulanger, M. J., Arase, H., Lanier, L. L., and Garcia, K. C. (2007) *Proc. Natl. Acad. Sci. U. S. A.* **104,** 10128–10133
19. Mathys, S., Schroeder, T., Ellwart, J., Koszinowski, U. H., Messerle, M., and Just, U. (2003) *J. Infect. Dis.* **187,** 988–999
20. Otwinowski, Z., and Minor, W. (1997) *Methods Enzymol.* **276,** 307–326
21. Adams, P. D., Grosse-Kunstleve, R. W., Hung, L. W., Ioerger, T. R., McCoy, A. J., Moriarty, N. W., Read, R. J., Sacchettini, J. C., Sauter, N. K., and Terwilliger, T. C. (2002) *Acta Crystallogr. D. Biol. Crystallogr.* **58,** 1948–1954
22. Emsley, P., and Cowtan, K. (2004) *Acta Crystallogr. D. Biol. Crystallogr.* **60,** 2126–2132
23. Read, R. J. (2001) *Acta Crystallogr. D. Biol. Crystallogr.* **57,** 1373–1382
24. Murshudov, G. N., Vagin, A. A., and Dodson, E. J. (1997) *Acta Crystallogr. D. Biol. Crystallogr.* **53,** 240–255
25. Painter, J., and Merritt, E. A. (2005) *Acta Crystallogr. D. Biol. Crystallogr.* **61,** 465–471
26. Brunger, A. T., Adams, P. D., Clore, G. M., DeLano, W. L., Gros, P., Grosse-Kunstleve, R. W., Jiang, J. S., Kuszewski, J., Nilges, M., Pannu, N. S., Read, R. J., Rice, L. M., Simonson, T., and Warren, G. L. (1998) *Acta Crystallogr. D. Biol. Crystallogr.* **54,** 905–921
27. Berman, H. M., Westbrook, J., Feng, Z., Gilliland, G., Bhat, T. N., Weissig, H., Shindyalov, I. N., and Bourne, P. E. (2000) *Nucleic Acids Res.* **28,** 235–242
28. DeLano, W. L. (ed) (2002) *The PyMOL User's Manual*, DeLano Scientific, Palo Alto, CA
29. Schuck, P. (2000) *Biophys. J.* **78,** 1606–1619
30. Allen, H., Fraser, J., Flyer, D., Calvin, S., and Flavell, R. (1986) *Proc. Natl. Acad. Sci. U. S. A.* **83,** 7447–7451
31. Townsend, A., Ohlen, C., Foster, L., Bastin, J., Ljunggren, H. G., and Karre, K. (1989) *Cold Spring Harbor Symp. Quant. Biol.* **54,** 299–308
32. Bjorkman, P. J., Saper, M. A., Samraoui, B., Bennett, W. S., Strominger, J. L., and Wiley, D. C. (1987) *Nature* **329,** 506–512
33. Halaby, D. M., and Mornon, J. P. (1998) *J. Mol. Evol.* **46,** 389–400
34. Holm, L., and Sander, C. (1996) *Science* **273,** 595–603
35. Fremont, D. H., Matsumura, M., Stura, E. A., Peterson, P. A., and Wilson, I. A. (1992) *Science* **257,** 919–927
36. Burmeister, W. P., Gastinel, L. N., Simister, N. E., Blum, M. L., and Bjorkman, P. J. (1994) *Nature* **372,** 336–343
37. Li, P., McDermott, G., and Strong, R. K. (2002) *Immunity* **16,** 77–86
38. Lawrence, M. C., and Colman, P. M. (1993) *J. Mol. Biol.* **234,** 946–950
39. Hu, C. D., Chinenov, Y., and Kerppola, T. K. (2002) *Mol. Cell* **9,** 789–798
40. Vink, C., Beuken, E., and Bruggeman, C. A. (2000) *J. Virol.* **74,** 7656–7665
41. Cosman, D., Fanger, N., Borges, L., Kubin, M., Chin, W., Peterson, L., and Hsu, M. L. (1997) *Immunity* **7,** 273–282
42. Wills, M. R., Ashiru, O., Reeves, M. B., Okecha, G., Trowsdale, J., Tomasec, P., Wilkinson, G. W., Sinclair, J., and Sissons, J. G. (2005) *J. Immunol.* **175,** 7457–7465
43. Alcami, A., and Koszinowski, U. H. (2000) *Trends Microbiol.* **8,** 410–418
44. Bowness, P. (2002) *Rheumatology* (*Oxford*) **41,** 857–868
45. Shiroishi, M., Kuroki, K., Ose, T., Rasubala, L., Shiratori, I., Arase, H., Tsumoto, K., Kumagai, I., Kohda, D., and Maenaka, K. (2006) *J. Biol. Chem.* **281,** 10439–10447
46. Smith, L. M., Shellam, G. R., and Redwood, A. J. (2006) *Virology* **352,** 450–465
47. Chenna, R., Sugawara, H., Koike, T., Lopez, R., Gibson, T. J., Higgins, D. G., and Thompson, J. D. (2003) *Nucleic Acids Res.* **31,** 3497–3500
48. Gouet, P., Courcelle, E., Stuart, D. I., and Metoz, F. (1999) *Bioinformatics* **15,** 305–308
49. Laskowski, R. A., Moss, D. S., and Thornton, J. M. (1993) *J. Mol. Biol.* **231,** 1049–1067